

Nature friendly single atom Pt catalyst for propane dehydrogenation

Saeed K. Amini*

*Chemistry and Chemical Engineering Research Center of Iran, Tehran, Iran

Received: 26 May 2025, Accepted: 2 August 2025

ABSTRACT

Activity of 111 surface of PtGa alloy in which three atom Pt centers are covered by In (indium) atoms was investigated as single atom Pt catalyst of propane dehydrogenation (PDH) by using quantum mechanical (QM) calculations. Periodic density functional theory (DFT) was applied in these calculations, utilizing PBE exchange-correlation functional with plane wave basis set of 680 eV kinetic energy cut off. Calculated results gave adsorption and conversion energies of propane to propylene including adsorption energies of intermediate states. Adsorption energies span was from -6 kJ/mole for propane up to -500 kJ/mole for $\text{CH}_3\text{CH}_2\text{CH}_2$ radical. Catalyzed propane to propylene's conversion energy was about -135 kJ/mole in comparison to about 150 kJ/mole of gas phase. Moderate adsorption energy value of about -120 kJ/mole for propylene and its higher conversion energy value of about 160 kJ/mole to $\text{CH}_3\text{CH}^*\text{CH}_2$ intermediate guarantee propylene selectivity and break of conversion chain after its formation. The lower activation energy values of the first and second C-H breaks indicate that the PDH reaction on this proposed catalyst is much faster than the previously reported catalyst in which the three platinum atom centers were covered by toxic Pb atoms. **Polyolefins J (2025) 12: 203-211**

Keywords: PDH; single atom catalyst; PtGa/In; QM; plane wave.

INTRODUCTION

As the second important produced feedstock of petrochemical industries next to ethylene, propylene is the main precursor in production of many of chemical materials that are used in industrial and domestic units. Importance of its production is so high that despite economic emergence due to coronavirus pandemic in 2020, its production rate passed 116 million tons. As its industrial production was started from 70 years ago, this high level of production rate is due to its different consumption types for many years. Bell *et al.*

have reported its weight percent production rate from different methods in 2016 and predicted demand up to 2021 (Supporting Figures 1 and 2, respectively) [1]. These figures show that an increasing gap was formed between its demand and supply values from 2007 [1]. They also show that about 80 percent of consumed propylene around the world is byproduct of catalysis and steam cracking industrial units which are designated for ethylene production [1]. Since its demand growth rate is higher than that of ethylene, the use of other methods

*Corresponding Author - E-mail: amini_s@ccerci.ac.ir

of propylene production is inevitable. According to these figures, two most selective methods for propane production by more than 50% selectivity towards propylene are propane dehydrogenation (PDH) and advance methane to olefin (MTO) processes [1].

Selectivity of PDH towards propylene exceeds 85% that makes it the highest weight percent yield method of propylene production [1]. This reaction is possible via oxidative and non-oxidative processes [2]. Non-oxidative process which employs heterogeneous catalysts is exploited more than oxidative process because oxidative process suffers from less selectivity toward propylene production. Selectivity and stability of catalysts of non-oxidative process are determined via balancing between desorption of produced propylene and its involvement in undesirable side reactions such as cracking of next C–H(C) bonds and following coke production. In the Pt-based catalysts, the Pt-Pt ensembles are known as active sites for undesirable dehydrogenation of propylene and its hydrogencraft. Thus, isolation of Pt atoms from each other on the catalyst's surface is an efficient method for inhibition from these undesirable side reactions. To this end, some novel studies report use of single atom like Pt catalysts for PDH in which Pt-Pt ensembles are absent [3-17]. Concurrently, many other single atom catalysts have been reported for this reaction [17-27].

Nakaya *et al.* tried to improve the selectivity of PtGa alloy catalyst by covering its undesirable multi platinum centers via deposition of some metallic atoms [14]. They isolated the Pt atoms of silica-supported PtGa catalyst from each other by Pb deposition. By using different Pt/Pb weight ratios, they produced a catalyst including isolated single Pt atoms which was nominated as single atom Pt catalyst [14]. It was stable for at least 96 hours at 600°C with 96.6% of selectivity towards propylene and 30% of propane conversion. By using just one Pt/In weight ratio, they stated that the use of indium instead of lead did not lead to more favorable results [14]. They state this result in the context that, despite extensive studies on various lead-covered catalysts, they have reported only one study on an indium (In)-covered catalyst with a platinum to indium weight ratio of 2, without any computational effort [14]. Interestingly and according to Peer Review File of that article, reviewers did not ask for any more explanation about indium-covered catalyst [14]. These evidences show that use of other Pt/In weight ratios may result in more favorable indium-covered PtGa

catalyst than those of Pb-covered catalyst.

Meanwhile, these atoms' isolations in laboratory and experimental conditions are such hard jobs that limit more surveys about these situations and improvement of their precisions. To this end, reported experimental data are very limited in these cases and one does not have much experimental data for comparison. Computational methods of chemistry have been employed in many PDH studies, specially from 2020, because of the omission of many high-priced and time consuming experimental assessments of proposed catalysts [14-16, 18, 28-52]. Because these methods can easily model the isolated single atom catalysts, most new PDH surveys benefit from computational methods alongside their experimental analyses to investigate and improve activity of catalysts [7-21, 51-58].

By considering the mentioned drawbacks of Nakaya *et al.*'s study about In-covered PtGa catalyst and efficiencies of computational chemistry methods, it encourages to investigate computationally this catalyst [14]. High value findings of this study will remove problems with the use of Pb and introduce a less hazardous catalyst [14]. After confirming this catalyst by computational method, the search for the PDH reaction mechanism on it was carried out by comparing the obtained reaction variables with the four accepted Langmuir-Hinshelwood mechanisms [49].

EXPERIMENTAL

Computational Details

It was tried to follow Nakaya *et al.*'s computational strategy in this study because the aim of this research was the survey of PDH on single atom PtGa/In catalyst by comparison of its characteristics and activity with that of PtGa/Pb [14]. To this end, the 111 surface of a cluster of PtGa crystal, covered with In atoms, was primarily used as an input structure which includes 100 atoms (Figure 1) [59]. Crystal space group is the first structural parameter that should be set at the beginning of a periodic quantum mechanical calculations. In spite of PtGa alloy that has given cubic P2/3 space group, addition of In atoms on its 111 surface changes its space group to triclinic P1 [59]. Dimensions of central unit cell in periodic quantum mechanical calculations with this space group in the *x* and *y* directions were

set to 12.18Å and 7.03Å, respectively. Dimension of z direction was set to 30Å in order to avoid interaction between adsorption slabs in this direction. All of the three α , β and γ angles were set to 90° according to triclinic P1 space group. The three atom Pt centers in the z direction were inhibited from catalysis by covering each of them by an In atom. The single atom Pt centers were held uncovered in the z direction as adsorption and reaction centers that only one of them was used as adsorption and reaction center in input file. Considering hexagonal structure of Pt centers on 111 surface of PtGa alloy, this arrangement inhibits interaction among adsorbed species with each other because remaining three single atom Pt centers of this central unit cell and their three images in neighboring unit cells surround this reaction center. They also can assist it, if adsorbates either move on the surface during geometry optimization or break to several parts that need extra adsorption centers.

The PBE exchange-correlation functional with plane wave basis set of 680eV kinetic energy cut off was applied as computational level of theory. Fermi dispersion index and convergence indexes of energy fluctuations, single electron orbital and ion position were set to 0.1eV, 1.0×10^{-10} , 1.0×10^{-8} and 1.0×10^{-8} , respectively. The cut off radius for interaction calculation by Ewald algorithm was set to 3Å. Because of hardware limitations and use of NWChem instead of Nakaya *et al.*'s use of CASTEP, it was not possible to set all the computational parameters as similar as each other [60,61]. In order to apply Van der Waals interactions in NWChem, the vdw3 correction was applied.

Crystal symmetry of geometry optimized structures

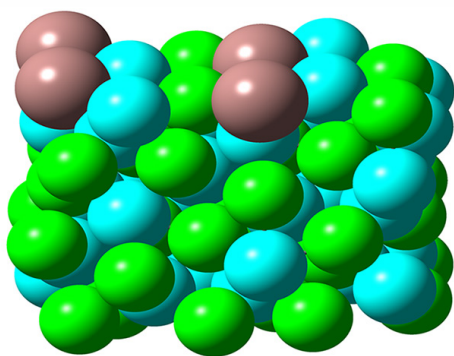


Figure 1. The 111 surface of PtGa crystal as single atom Pt catalyst in which three atom Pt centers are covered by In atoms [59]. The blue, green and brown colors refer to Pt, Ga and In atoms, respectively.

was distorted and different from input structures when dimensions of central unit cell were optimized in accordance with Nakaya *et al.*'s article. This is due to implementation of the lowest level of symmetry for crystal structure that states a higher level of crystal symmetry should be enforced if it is possible.

In order to apply a higher level of symmetry on crystal structure, the applicable hexagonal P6₃/mmc space groups were employed by special choice of atoms in the x and y directions. These space groups were selected because they are consistent with hexagonal structure of Pt centers. On the other hand, one can produce several similar slabs with large distances in z direction by setting its dimension to a large value and survey PDH reaction by seating propane on these layers. Dimensions of the central unit cell in the x, y and z directions were set to 7.03, 7.03 and 100Å, respectively. The γ angle was set to 120°. Because these space groups consider several layers in calculations instead of one layer of P1 space group, computational time was increased so much that caused to calculations' corruption due to hardware resource limitations. Thus, the number of atomic layers of the structure of Figure 1 was halved and the number of atoms was decreased to 50 atoms from previous 100 atoms.

RESULTS AND DISCUSSION

Two main steps of a periodic quantum mechanical calculation are adjustment of *k*-point meshes and energy cut off values for accurate sampling of Brillouin zone and precise determining of plane waves' energies, respectively. To this end, catalyst structure without adsorbed species was subject to geometry optimization with different *k*-point meshes and energy cut off values. Summarized results of these calculations in Table 1 show that due to the use of large number of atoms in central unit cell, their changes have no significant effect on the energy of catalyst. Thus, $1 \times 1 \times 1$ *k*-point mesh with 70Ry energy cut off values are obtained as optimized variables that may be used in subsequent calculations. Meanwhile, due to better proficiency reported for $3 \times 3 \times 3$ *k*-point mesh in literature, it was employed in subsequent calculations. As the energy of catalyst was decreased by increasing the energy cut off from 20 to 70Ry, it was concluded that cut off values larger than 70Ry are

Table 1. Energies of optimized geometries of adsorbate free PtGa/In catalyst with different k -point mesh and energy cut off values.

Energy Cut Off (Ry)	k -point mesh	Energy of optimized geometry (Hartree)
20	1×1×1	-785.858256
20	3×3×3	-785.968263
30	3×3×3	-786.051143
40	3×3×3	-786.113021
45	3×3×3	-786.164236
50	3×3×3	-786.206193
55	3×3×3	-786.216573
60	3×3×3	-786.219742
70	3×3×3	-786.221856

necessary to have convergence. Meanwhile, according to literatures, energy cut off values larger than 700eV cause severe errors in computational results and are not recommended. On the other hand, due to the very small difference between catalyst energies of calculations with 50 and 70Ry cut off values and considering very different spent computer time for these calculations, the 50Ry or 680eV was selected as the optimized cut off value in subsequent calculations.

By reaching optimized values for k -point mesh and cut off value, propane, propylene and corresponding radicals and intermediates were deposited over catalyst to run subsequent quantum mechanical calculations using these complexes of adsorbates and adsorbents. Most probable orientations of propane, propylene and their related counterparts, such as radicals and intermediate states, on the 111 surface of GaPt catalyst in which three Pt atom catalyst centers were covered by In atoms were constructed as input structures for geometry optimization calculations. Up and side views of these input structures are summarized in Figure 2. Output geometries of these optimizations determine the resulting transition states' and products' structures, reaction rate and its mechanism. In order to obtain real optimized geometries that are free from any applied constraints on angles and bond lengths of adsorbed species, geometries of adsorbate-adsorbent complexes were optimized by fixing just two inferior Pt and two inferior Ga layers of catalyst. For example, the activated $\text{CH}_3\text{CH}_2\text{CH}_2\text{H}^*$ and $\text{CH}_3\text{CH}^*\text{HCH}_2$ structures, in which C—H bonds of * recognized hydrogen atoms were elongated in input structure, were optimized without any constraint on activated bonds. Similar to optimized structures of adsorbate free catalyst, indium atoms of geometry optimized structures of these complexes remain in their initial

positions that supports catalyst persistence against distortion during geometry optimization. Figure 2 includes top and side views of the structures resulting from geometry optimization calculations alongside the input structures. In the optimized structures of all species including CH_3CHCH_2 and $\text{CH}_3\text{CH}_2\text{CH}_3$ molecules, $\text{CH}_3\text{CH}_2\text{CH}_2\text{H}^*$, $\text{CH}_3\text{CHH}^*\text{CH}_2$ and $\text{CH}_3\text{CH}^*\text{CH}_2$ intermediates and $\text{CH}_3\text{CH}_2\text{CH}_2$ radical on the single atom Pt catalytic center, they remain adsorbed on the catalyst surface which reflect their efficient adsorption against addition of indium atoms.

In order to obtain the energy changes in going from reactants to products, energy of catalyst of any complex without corresponding adsorbate and the energy of

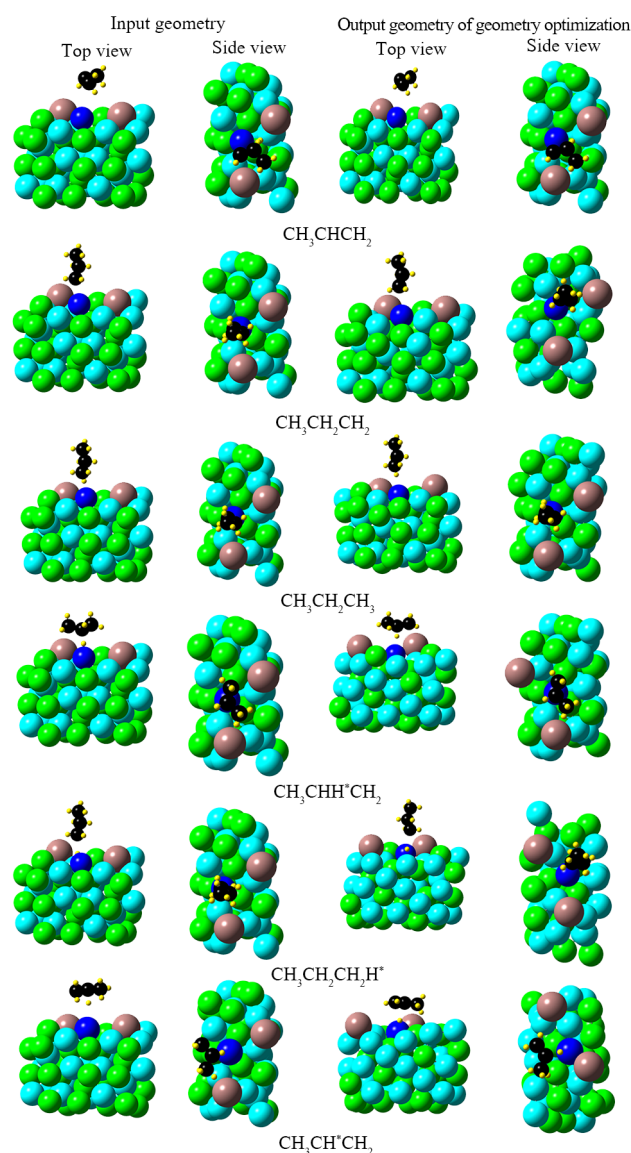


Figure 2. Side and top views of input and geometry optimized output geometries of adsorbates on PtGa/In catalyst. The blue, dark blue, green and brown colors refer to Pt, single atom Pt center, Ga and In atoms, respectively.

Table 2. Energies of catalyst of any structure without adsorbates and adsorbates of that structure without catalyst were calculated by using optimized geometries of adsorbates+catalyst structures. All in Hartree/species except to adsorption of output structure values that are in kJ/mole.

Structure	Total	Catalyst	Output structure	Adsorption of output structure
CH_3CHCH_2	-806.7797590	-786.175672	-20.64905496	-118.06
$\text{CH}_3\text{CH}_2\text{CH}_2$	-807.5839912	-786.177345	-21.21543835	-502.02
$\text{CH}_3\text{CH}_2\text{CH}_3$	-808.0680869	-786.191253	-21.87461240	-5.83
$\text{CH}_3\text{CHH}^*\text{CH}_2$	-807.5472561	-786.180426	-21.19424523	-453.12
$\text{CH}_3\text{CH}_2\text{CH}_2\text{H}^*$	-808.0737856	-786.189852	-21.86253412	-56.18
$\text{CH}_3\text{CH}^*\text{CH}_2$	-806.6185625	-786.184182	-20.40864523	-67.57

any adsorbate of that complex without corresponding catalyst were calculated by using optimized geometries of corresponding adsorbates+catalyst complexes (left column of Figure 2). These energies along with the total energies of corresponding complexes are summarized in Table 2 in Hartree/molecule because their conversion to kJ/mole makes very large digits. Of course, adsorption energies of adsorbates of corresponding complexes are summarized in this table in kJ/mole. This table shows that molecular adsorption of propylene on the single atom Pt center has a moderate adsorption energy value of -118.06 kJ/mole which is comparable with -108.3 kJ/mole of PtGa/Pb [14]. Significant difference between adsorption energies of molecular propane and propylene species reflects metal- Π interaction in the propylene which causes higher adsorption energy value in this case. Very high adsorption energy values of 7H species of $\text{CH}_3\text{CH}_2\text{CH}_2$ radical and $\text{CH}_3\text{CH}^*\text{HCH}_2$ intermediate reflect the existence of unpaired electrons in these cases. This conclusion is certified by the moderate adsorption energies of 6H and 8H intermediates of $\text{CH}_3\text{CH}_2\text{CH}_2\text{H}^*$ and $\text{CH}_3\text{CH}^*\text{CH}_2$ in which there is coupling between unpaired electrons of elongated H* atom and parental segment.

Conversion energies of reactants to products in kJ/mole which are obtained by using data of Table 2 are summarized in Table 3. These values that imply their energy differences over catalyst are obtained by subtracting the adsorption energy of each species and the corresponding bare catalyst's energy from the total energy of their complex. This table also includes gas phase calculations data for comparison. Despite gas phase calculation in which formation of propylene from propane is 147.6 kJ/mole endothermic, this reaction is exothermic on the catalyst surface in $\text{CH}_3\text{CH}_2\text{CH}_2\text{H}^*$ and $\text{CH}_3\text{CH}_2\text{CH}_3$ adsorption states by -98.9 and -134.3 kJ/mole, respectively. Meanwhile, conversion of $\text{CH}_3\text{CHH}^*\text{CH}_2$ and $\text{CH}_3\text{CH}_2\text{CH}_2$ species to propylene on the catalyst are endothermic by 118.3

and 70.7 kJ/mole, respectively. On the other hand, adsorption energies of seven hydrogen species with unpaired electron are so high that their conversion to propylene by leaving an adsorbed radical H cannot compensate it.

Reaction coordinate of PDH is summarized in Figure 3. Due to higher activation energies of the first and second transition states in proposed In-covered PtGa catalyst, it shows less activity relative to Pt single-atom, Pt4 and Pt3Sn single-cluster catalysts, all supported on g- C_3N_4 [55]. Due to the very high adsorption energies of seven hydrogen species on this catalyst, their formation from eight hydrogen species is about 653-835 kJ/mole exothermic that release of their energies warrants supply of necessary energies for activation and conversion of $\text{CH}_3\text{CH}_2\text{CH}_3$ molecule to them and following cleavage of a hydrogen atom and propylene formation. This conclusion is certified by 77 kJ/mole released energy for propane conversion to $\text{CH}_3\text{CH}_2\text{CH}_2\text{H}^*$ intermediate. On the other hand, it gives much higher activity relative to Pt doped Cr_2O_3 , PtGe, Pt/Cu, Pt₃Cu, Pt(111), Sn₁Pt, Pt₁-S4/edge, Pt single atom of PtGa, Pt₃Sn single-cluster supported on Al_2O_3 and Pt3Sn(111) catalysts because of its very lower first and second transition states' energy barriers

Table 3. Conversion energies of reactants to products in kJ/mole.

Reactant	Product	Conversion Energy	Gas Phase
$\text{CH}_3\text{CH}_2\text{CH}_3$	CH_3CHCH_2	-134.26	147.61
$\text{CH}_3\text{CH}_2\text{CH}_2\text{H}^*$		-98.87	
$\text{CH}_3\text{CH}_2\text{CH}_2$		70.74	
$\text{CH}_3\text{CHH}^*\text{CH}_2$		118.29	
$\text{CH}_3\text{CH}_2\text{CH}_3$	$\text{CH}_3\text{CH}_2\text{CH}_2$	799.03	
$\text{CH}_3\text{CH}_2\text{CH}_2\text{H}^*$		834.42	
$\text{CH}_3\text{CH}_2\text{CH}_3$	$\text{CH}_3\text{CHH}^*\text{CH}_2$	653.69	
$\text{CH}_3\text{CH}_2\text{CH}_2\text{H}^*$		689.08	
$\text{CH}_3\text{CH}_2\text{CH}_3$	$\text{CH}_3\text{CH}_2\text{CH}_2\text{H}^*$	76.98	
CH_3CHCH_2	$\text{CH}_3\text{CH}^*\text{CH}_2$	118.15	

[10-15, 57]. These results are summarized in Figure 3.

As Table 2 shows, the moderate adsorption energy of molecular propylene on In-covered PtGa is due to adsorption over single atom Pt center that shows a lower tendency towards adsorption of molecular propylene in comparison to three atom Pt centers. This moderate tendency towards propylene adsorption causes higher selectivity of catalyst towards propylene via faster desorption of produced propylene in comparison to more proceed of reaction by propylene cracking (Figure 3). Thus, it gives higher selectivity towards propylene relative to Pt single-atom, Pt₄ and Pt₃Sn single-cluster catalysts, all supported on g-C₃N₄, Pt₃Cu and Pt(111), due to faster desorption of propylene in comparison to its conversion to C₃H₅ [15,55]. Of course, it gives lower selectivity towards propylene relative to Pt/Cu and Pt single atom of PtGa catalysts due to their higher activation energy towards C₃H₅ [14,15].

These findings show that use of other Pt/In weight ratios results in higher activity of this catalyst relative to those of Pb which have not been reported by Nakaya *et al.* and corrects their data for precise In-covered catalyst [14].

Reaction mechanism of PDH on this catalyst can be guessed by comparing calculated kinetics data with those of PtSn₃/K catalyst, calculated by Farjoo *et al.* for the four most accepted Langmuire-Hinshelwood mechanisms [49,62]. Considering the -118 kJ/mole adsorption energy of propylene, the reaction mechanism is more compatible with model 3 of PtSn₃/K catalyst in which this step is rate determining

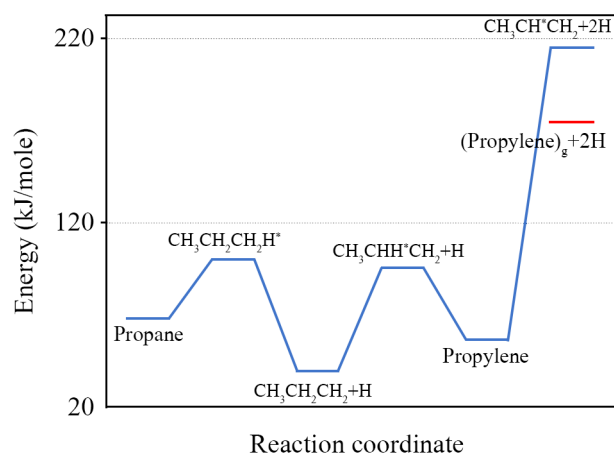


Figure 3. Energy diagram of PDH reaction. Hydrogen atoms recognized by asterisk have elongated bond lengths. All species are in adsorbed state except to recognized (Propylene)_g.

one (Supporting scheme 1) [62]. On the other hand, conversion energy of propane to propylene is obtained equal to -134 kJ/mole which is bigger than -71 kJ/mole of this model [62]. Thus, these calculations propose model 3 with higher rate constant than that of PtSn₃/K catalyst [62].

CONCLUSION

Calculated results show that reaction rate of PDH over PtGa catalyst in the presence of In is much faster than the values reported in the presence of Pb [14]. These calculations propose a single atom catalyst that beside its benefit from high selectivity of these sort of catalysts, has faster reaction rate and is free of toxic Pb element. Thus, it is recommended to repeat experiments in the presence of In in order to obtain more accurate results and survey this proposition.

CONFLICTS OF INTEREST

The authors declare that there are no conflicts of interest to disclose.

REFERENCES

1. Bell AT, Alger MM, Flytzani-Stephanopoulos M, Gunnoe TB, Lercher JA, Stevens J, Alper J, Tran C (2016) The changing landscape of hydrocarbon feedstocks for chemical production: Implications for catalysis. In: National academies of sciences, engineering, and medicine, Washington, DC, USA
2. Otroshchenko T, Jiang G, Kondratenko VA, Rodemerck U, Kondratenko EV (2021) Current status and perspectives in oxidative, non-oxidative and CO₂-mediated dehydrogenation of propane and isobutane over metal oxide catalysts. Chem Soc Rev 50: 473-527
3. Yang F, Zhang J, Chen J, Wang G, Yu T, Li Q, Shi Z, Sun Q, Zhuo R, Wang R (2024) Boosting propane dehydrogenation of defective S-1 stabilized single-atom Pt and ZnO catalysts via coordination environment regulation. Nano Res 17: 5884-5896
4. Nakaya Y, Furukawa S (2022) Tailoring single-

- atom platinum for selective and stable catalysts in propane dehydrogenation. *ChemPlusChem* 87: e202100560
5. Liu X, Wang X, Zhen S, Sun G, Pei C, Zhao Z, Gong J (2022) Support stabilized PtCu single-atom alloys for propane dehydrogenation. *Chem Sci* 13: 9537-9543
 6. Yang Y, Liu Q, Wang J, Li P, Miao C, Liu J, Yang Y, Wang J, Wang X (2024) Hydroxy- or chlorine-anchored Pt single-atom in Al_2O_3 : Which is better for propane dehydrogenation? *AIChE J* 70: e18288
 7. Dong C, Lai Z, Wang H (2023) Comprehensive mechanism and microkinetic model-driven rational screening of 3N-modulated single-atom catalysts for propane dehydrogenation. *ACS Catal* 13: 5529-5537
 8. Zhao Q, Chen L, Ma S, Liu Z (2025) Data-driven discovery of Pt single atom embedded germanosilicate MFI zeolite catalysts for propane dehydrogenation. *Nat Commun* 16: 372
 9. Lin J, Shen M, Zhang C, Bi S, Shen G, Gao F, Li W (2025) Active and stable platinum-indium single atom alloy catalysts for propane dehydrogenation. *Chem Eng J* 519 : 165243
 10. Xing Y, Kang L, Ma J, Jiang Q, Su Y, Zhang S, Xu X, Li L, Wang A, Liu Z, Ma S, Liu XY, Zhang T (2023) Sn1Pt single-atom alloy evolved stable PtSn/nano- Al_2O_3 catalyst for propane dehydrogenation. *Chinese J Catal* 48: 164-174
 11. Nakaya Y, Hayashida E, Asakura H, Takakusagi S, Yasumura S, Shimizu K, Furukawa S (2022) High-entropy intermetallics serve ultrastable single-atom Pt for propane dehydrogenation. *J Am Chem Soc* 144(35): 15944-15953
 12. Dong C, Lai Z, Wang H (2024) Design of MoS₂ edge-anchored single-atom catalysts for propane dehydrogenation driven by DFT and microkinetic modeling. *Phys Chem Chem Phys* 26: 5303-5310
 13. Jin D, Xu H, Zhu J, Cheng D (2023) Activation of Cr_2O_3 for propane dehydrogenation by doping with Pt single-atom promotor. *Mol Catal* 551: 113624
 14. Nakaya Y, Hirayama J, Yamazoe S, Shimizu K, Furukawa S (2020) Single-atom Pt in intermetallics as an ultrastable and selective catalyst for propane dehydrogenation. *Nat Commun* 11: 2838
 15. Sun G, Zhao Z, Mu R, Zha S, Li L, Chen S, Zang K, Luo J, Li Z, Purdy SC, Kropf AJ, Miller JT, Zeng L, Gong J (2018) Breaking the scaling relationship via thermally stable Pt/Cu single atom alloys for catalytic dehydrogenation. *Nat Commun* 9: 4454
 16. Marcinkowski MD, Darby MT, Liu J, Wimble JM, Lucci FR, Lee S, Michaelides A, Flytzani-Stephanopoulos M, Stamatakis M, Sykes ECH (2018) Pt/Cu single-atom alloys as coke-resistant catalysts for efficient C–H activation. *Nat Chem* 10: 325-332
 17. Xiong C, Dai S, Wu Z, Jiang D (2022) Single atoms anchored in hexagonal boron nitride for propane dehydrogenation from first principles. *ChemCatChem* 9(2022). *ChemCatChem* 14: e202200465
 18. Chang QY, Wang KQ, Sui ZJ, Zhou XG, Chen D, Yuan WK, Zhu YA (2021) Rational design of single-atom-doped Ga_2O_3 catalysts for propane dehydrogenation: Breaking through volcano plot by Lewis acid-base interactions. *ACS Catal* 11: 5135-5147
 19. Zhang W, Guo J, Ma H, Wen J, He C (2022) Anchoring of transition metals to CN as efficient single-atom catalysts for propane dehydrogenation. *Chem Phys Lett* 809: 140154
 20. Qu Z, He G, Zhang T, Fan Y, Guo Y, Hu M, Xu J, Ma Y, Zhang J, Fan W, Sun Q, Mei D, Yu J (2024) Tricoordinated single-atom cobalt in zeolite boosting propane dehydrogenation. *J Am Chem Soc* 146: 8939-8948
 21. Zhang Y, Shi S, Wang Z, Lan H, Liu L, Sun Q, Guo G, He X, Ji H (2024) Propane dehydrogenation on Ir single-atom catalyst modified by atomically dispersed Sn promoters in silicalite-1 zeolite. *AIChE J* 70: e18431
 22. Zhang Q, Jiang X, Su Y, Zhao Y, Qiao B (2024) Catalytic propane dehydrogenation by anatase supported Ni single-atom catalysts. *Chinese J Catal* 57: 105-113
 23. Ma R, Dean DP, Gao J, Wang M, Liu Y, Liang K, Wang J, Miller JT, Zhou B, Zou G, Kou J (2024) Lattice-embedded Ni single-atom catalyst on porous Al_2O_3 nanosheets derived from Ni-doped carbon dots for efficient propane dehydrogenation. *Appl Catal B- Environ Energy* 347: 123798
 24. Guo L, Shi D, Zhang T, Ma Y, Qi G, Xu J,

- Sun Q (2025) Unsaturated cobalt single-atoms stabilized by silanol nests of zeolites for efficient propane dehydrogenation. *Chinese J Catal* 72: 323-333
25. Kang L, Zhu B, Gu Q, Duan X, Ying L, Qi G, Xu J, Li L, Su Y, Xing Y, Wang Y, Li G, Li R, Gao Y, Yang B, Liu XY, Wang A, Zhang T (2025) Light-driven propane dehydrogenation by a single-atom catalyst under near-ambient conditions. *Nat Chem* 17: 890-896
 26. Chen J, Yue Y, Liu W (2025) Harnessing light for propane dehydrogenation: a single-atom catalyst milestone achieved under mild conditions. *Sci China Chem* 68: 2776-2778
 27. Chernov AN, Sobolev VI, Gerasimov EY, Koltunov KY (2022) Propane dehydrogenation on Co-N-C/SiO₂ catalyst: The role of single-atom active sites. *Catalysts* 12: 1262
 28. Cao L, Dai P, Zhu L, Yan L, Chen R, Liu D, Gu X, Li L, Xue Q, Zhao X (2020) Graphitic carbon nitride catalyzes selective oxidative dehydrogenation of propane. *Appl Catal B-Environ* 262: 118277
 29. Huš M, Kopač D, Likozar B (2020) Kinetics of non-oxidative propane dehydrogenation on Cr₂O₃ and the nature of catalyst deactivation from first-principles simulations. *J Catal* 386: 126-138
 30. Chen S, Pei C, Chang X, Zhao Z, Mu R, Xu Y, Gong J (2020) Coverage-dependent behaviors of vanadium oxides for chemical looping oxidative dehydrogenation. *Angew Chem Int Ed* 59: 22072-22079
 31. Wang P, Senftle TP (2021) Theoretical insights into non-oxidative propane dehydrogenation over Fe₃C. *Phys Chem Chem Phys* 23: 1401-1413
 32. Wang T, Cui X, Winther KT, Abild-Pedersen F, Bligaard T, Nørskov JK (2021) Theory-aided discovery of metallic catalysts for selective propane dehydrogenation to propylene. *ACS Catal* 11: 6290-6297
 33. Xie Z, Li Z, Tang P, Song Y, Zhao Z, Kong L, Fan X, Xiao X (2021) The effect of oxygen vacancies on the coordinatively unsaturated Al-O acid-base pairs for propane dehydrogenation. *J Catal* 397: 172-182
 34. Liu J, Luo W, Yin Y, Fu X, Luo J (2021) Understanding the origin for propane non-oxidative dehydrogenation catalysed by d2-d8 transition metals. *J Catal* 396: 333-341
 35. Sun X, Xue J, Ren Y, Li X, Zhou L, Li B, Zhao Z (2021) Revealing nature of active site and reaction mechanism of supported chromium oxide catalyst in propane direct dehydrogenation. *Mol Catal* 505: 111520
 36. Sharma L, Jiang X, Wu Z, Baltrus J, Rangarajan S, Baltrusaitis J (2021) Elucidating the origin of selective dehydrogenation of propane on γ -alumina under H₂S treatment and co-feed. *J Catal* 394: 142-156
 37. Castro-Fernández P, Mance D, Liu C, Moroz IB, Abdala PM, Pidko EA, Copéret C, Fedorov A, Müller CR (2021) Propane dehydrogenation on Ga₂O₃-based catalysts: Contrasting performance with coordination environment and acidity of surface sites. *ACS Catal* 11: 907-924
 38. Ye C, Peng M, Cui T, Tang X, Wang D, Jiao M, Miller JT, Li Y (2023) Revealing the surface atomic arrangement of noble metal alkane dehydrogenation catalysts by a stepwise reduction-oxidation approach. *Nano Res* 16: 4499-4505
 39. Xiao L, Shan Y, Sui Z, Chen D, Zhou X, Yuan W, Zhu Y (2020) Beyond the reverse Horiuti-Polanyi mechanism in propane dehydrogenation over Pt catalysts. *ACS Catal* 10: 14887-14902
 40. Araujo-Lopez E, Vandegehuchte BD, Curulla-Ferré D, Sharapa DI, Studt F (2020) Trends in the activation of light alkanes on transition-metal surfaces. *J Phys Chem C* 124: 27503-27510
 41. Abdelgaid M, Dean J, Mpourmpakis G (2020) Improving alkane dehydrogenation activity on γ -Al₂O₃ through Ga doping. *Catal Sci Technol* 10: 7194-7202
 42. Wang Z, Chen Y, Mao S, Wu K, Zhang K, Li Q, Wang Y (2020) Chemical insight into the structure and formation of coke on PtSn alloy during propane dehydrogenation. *Adv Sustain Syst* 4: 2000092
 43. Fan X, Liu D, Sun X, Yu X, Li D, Yang Y, Liu H, Diao J, Xie Z, Kong L (2020) Mn-doping induced changes in Pt dispersion and Pt_xMn_y alloying extent on Pt/Mn-DMSN catalyst with enhanced propane dehydrogenation stability. *J Catal* 389: 450-460
 44. Liu Z, Li Z, Li G, Wang Z, Lai C, Wang X, Pidko EA, Xiao C, Wang F, Li G (2020) Single-

- atom Pt⁺ derived from the laser dissociation of a platinum cluster: Insights into nonoxidative alkane conversion. *J Phys Chem Lett* 11: 5987-5991
45. Li A, Tian D, Zhao Z (2020) DFT studies on the reaction mechanism for the selective oxidative dehydrogenation of light alkanes by BN catalysts. *New J Chem* 44: 11584-11592
 46. Chang Q, Wang K, Hu P, Sui Z, Zhou X, Chen D, Yuan W, Zhu Y (2020) Dual-function catalysis in propane dehydrogenation over Pt₁-Ga₂O₃ catalyst: Insights from a microkinetic analysis. *AIChE J* 66: e16232
 47. Aly M, Fornero EL, Leon-Garzon AR, Galvita VV, Saeys M (2020) Effect of boron promotion on coke formation during propane dehydrogenation over Pt/ γ -Al₂O₃ catalysts. *ACS Catal* 10: 5208-5216
 48. Purdy SC, Ghanekar P, Mitchell G, Kropf AJ, Zemlyanov DY, Ren Y, Ribeiro F, Delgass WN, Greeley J, Miller JT (2020) Origin of electronic modification of platinum in a Pt₃V alloy and its consequences for propane dehydrogenation catalysis. *ACS Appl Energy Mater* 3:1410-1422
 49. Fogler H (1999) Elements of chemical reaction engineering, 3rd Ed. In.: Prentice Hall International, Inc, New Jersey.
 50. Zhang T, Lang X, Dong A, Wan X, Gao S, Wang L, Wang L, Wang W (2020) Difference of oxidation mechanism between light C₃-C₄ alkane and alkene over mullite YMn₂O₅ oxides catalyst. *ACS Catal* 10: 7269-7282
 51. Ma F, Chang QY, Yin Q, Sui ZJ, Zhou XG, Chen D, Zhu YA (2020) Rational screening of single-atom-doped ZnO catalysts for propane dehydrogenation from microkinetic analysis. *Catal Sci Technol* 10: 4938-4951
 52. Zhang J, Zhou RJ, Chang QY, Sui JZ, Zhou XG, Chen D, Zhu YA (2021) Tailoring catalytic properties of V₂O₃ to propane dehydrogenation through single-atom doping: A DFT study. *Catal Today* 368: 46-57
 53. Chen S, Chai Y, Chen Y, Wei F, Pan X, Lin J, Lin S (2024) Peripheral P doping in Zn₁/NC single-atom catalyst to enhance propane dehydrogenation reaction. *Chem Eng Sci* 291: 119919
 54. Wei F, Cao L, Ge B, Chen Y, Pan X, Chai Y, Jing R, Hu X, Wang X, Lin J, Lin S (2025) Regulating peripheral nitrogen dopants in single-atom catalysts to enhance propane dehydrogenation. *Angew Chem* 137: e202416912
 55. Pan J, Strugovshchikov E, Salóm-Català A, Novell-Leruth G, Kaźmierczak K, Curulla-Ferré D, Carbó JJ, Godard C, Ricart JM (2025) Propane dehydrogenation on Pt single-atom and Pt₄ and Pt₃Sn single-cluster supported on g-C₃N₄: A theoretical study. *J Phys Chem C* 129: 2477-2487
 56. Song W, Kang Y, Yang M, Li Z, Chen L, Zhao Z, Liu J (2022) Promoting propane dehydrogenation via strain engineering on iridium single-atom catalyst. *Fuel* 311: 122580
 57. Sun S, Sun G, Pei C, Zhao Z, Gong J (2021) Origin of performances of Pt/Cu single-atom alloy catalysts for propane dehydrogenation. *J Phys Chem C* 125: 18708-18716
 58. Hannagan RT, Giannakakis G, Réocreux R, Schumann J, Finzel J, Wang Y, Michaelides A, Deshlahra P, Christopher P, Flytzani-Stephanopoulos M, Stamatakis M, Sykes ECH (2021) First-principles design of a single-atom-alloy propane dehydrogenation catalyst. *Science* 372: 1444-1447
 59. Bhargava M, Gadalla A, Schubert K (1975) Koexistente Phasen vom FeSi-Typ in den Mischungen Ni-Pd-Ga und Ni-Pt-Ga. *J Less-Common Met* 42: 69-76
 60. Segall MD, Lindan PJD, Probert MJ, Pickard CJ, Hasnip PJ, Clark SJ, Payne MC (2002) First-principles simulation: ideas, illustrations and the CASTEP code. *J Phys Condens Matter* 14: 2717-2744
 61. Valiev M, Bylaska EJ, Govind N, Kowalski K, Straatsma TP, Van Dam HJ, Wang D, Nieplocha J, Apra E, Windus TL, de Jong W (2010) NWChem: A comprehensive and scalable open-source solution for large scale molecular simulations. *Comput Phys Commun* 181: 1477-1489
 62. Farjoo A, Khorasheh F, Niknaddaf S, Soltani M (2011) Kinetic modeling of side reactions in propane dehydrogenation over Pt - Sn/ γ - Al₂O₃ catalyst. *Sci Iran* 18: 458-464